Utilization of Estimated Sea Surface Wind Data Based on Himawari-8/9 Low-level AMVs for Tropical Cyclone Analysis

KENICHI NONAKA[1], SHUJI NISHIMURA[2] and YOHKO IGARASHI[2]
[1]Meteorological Satellite Center, Japan Meteorological Agency
[2]Tokyo Typhoon Center, Forecast Department, Japan Meteorological Agency

1. Introduction

The availability of sea surface wind information is important for application in determining areas with wind speeds exceeding 30 and 50 knots around tropical cyclones (TCs). However, wind data from observations over ocean areas are particularly sparse. The Advanced Scatterometer (ASCAT) on board the Metop series of satellites provides data on horizontal equivalent neutral wind at 10 m height (OSI SAF/EARS 2016), which is used as a major ancillary resource in TC analysis. ASCAT provides wind distribution information over a much wider area than in-situ observation platforms such as vessels and buoys, but its observation frequency is insufficient for TC monitoring.

Atmospheric motion vectors (AMVs) derived by tracking clouds in successive satellite images are utilized as a major source of observation-based wind information for data assimilation in numerical weather prediction (NWP). In particular, AMVs derived from geostationary satellite imagery provide frequent and wide-ranging wind distribution information for ocean areas. It is known that low-level AMVs, which are assigned to lower altitudes, have a strong correlation with in-situ sea surface observation wind data in the vicinity of TCs (e.g., Ohshima et al. 1991). Dunion and Velden (2002a) reported on the validation of surface wind data adjusted from GOES low-level cloud-drift wind data with a planetary boundary layer model via comparison with in-situ observations, and showed that low-level AMVs are valuable in analyzing wind fields around TCs. The Meteorological Satellite Center of the Japan Meteorological Agency (JMA/MSC) has also executed feasibility studies on sea surface wind estimation around TCs using low-level AMVs. The results of previous studies showed that Himawari-8 low-level AMVs have a strong correlation with sea surface wind data for areas around TCs, and can be used for sea surface wind estimation based on simple regression analysis.

Since July 2017, AMV-based sea-surface wind data (referred to here as “ASWinds”) derived from Himawari-8/9 low-level AMVs have been provided to the RSMC Tokyo – Typhoon Center and utilized for TC monitoring over the western North Pacific. Himawari-8 ASWinds were validated via comparison with sea surface wind data derived from ASCAT information (referred to here as “ASCAT winds”) in the vicinity of TCs

occurring in 2016.

This report details results obtained from validation of Himawari-8 ASWinds against ASCAT winds and their usage by the RSMC Tokyo – Typhoon Center. Section 2 details Himawari-8/9's low-level AMVs and estimation of ASWinds, Section 3 reports on the accuracy and characteristics of ASWinds in comparison with ASCAT winds, Section 4 presents examples of ASWinds usage in TC analysis, and Section 5 summarizes the report.

2. Himawari-8/9 low-level AMVs and sea surface winds around TCs

2.1. Himawari-8/9 and low-level AMVs

JMA's Himawari-8 geostationary meteorological satellite began observation on 7 July 2015, and Himawari-9 has been in standby operation as back-up since 2017. Both satellites are scheduled to continue observation until 2029, providing significantly enhanced imagery in terms of the number of observable spectral bands and tempo-spatial resolution compared with that of JMA's previous MTSAT-1R/2 satellites. The Advanced Himawari Imager (AHI) on board Himawari-8/9 has 16 spectral bands with wavelengths ranging from visible to infrared, and produces full-disk scans (yielding imagery of the whole earth as seen from the satellite) every 10 minutes as well as scans of four regional areas (the Japan area, a target area and two landmark areas) every 2.5 minutes (Bessho et al. 2016). The Himawari-8/9 AHI observable spectral bands and specifications are shown in Table 1. Spatial resolution, which depends on wavelength, is 0.5 km for visible band B03 (0.64 μm) and 2 km for infrared bands at the sub-satellite point (SSP).

JMA/MSC developed a new AMV derivation algorithm for the utilization of Himawari-8/9 enhanced satellite imagery (Shimoji 2016). Himawari-8/9 AMV derivation involves the main processes of motion vector calculation, height assignment for derived vectors, and quality control. Motion vectors are calculated by tracking the same target cloud patterns across three consecutive satellite images based on a cross-correlation method. In the height assignment process, an optimal estimation method is applied and the heights of motion vectors are derived by minimizing differences between observed and assumed (from an atmospheric vertical profile of JMA's global NWP model (GSM)) values of infrared radiances and derived motion vectors. In the quality control process, low-quality AMVs are filtered out in a series of checks, and the quality indicator (QI) developed at EUMETSAT (Holmlund 1998) is attached.

Table 1. Specifications of Himawari-8/9 AHI observation bands and spatial resolutions

	Band #		Central wave length [μm] Himawari-8	Himawari-9	Spatial resolution (@ssp) [km]
Visible	B01		0.47	0.47	1
	B02		0.51	0.51	
	B03	**VIS**	**0.64**	**0.64**	**0.5**
Near-infrared	B04		0.86	0.86	1
	B05		1.6	1.6	2
	B06		2.3	2.3	
Infrared	**B07**	**Shortwave IR (SWIR)**	**3.9**	**3.8**	**2**
	B08		6.2	6.2	
	B09		6.9	7.0	
	B10		7.3	7.3	
	B11		8.6	8.6	
	B12		9.6	9.6	
	B13	**IR**	**10.4**	**10.4**	
	B14		11.2	11.2	
	B15		12.4	12.4	
	B16		13.3	13.3	

Table 2. Specifications of Himawari-8/9 AMVs used for ASWinds

	Full-disk			Target observation		
	VIS (B03)	SWIR (B07)	IR (B13)	VIS (B03)	SWIR (B07)	IR (B13)
Target size (@ssp)	14 km			2.5 km	10 km	
Grid interval (@ssp)	18 km			3.5 km	3.5 km	
Image time interval	10 min.			2.5 min.	5 min.	
Derivation time	Every 30 min.			Every 10 min.		
Assigned height	> 700 hPa			> 700 hPa		

Visible and infrared window satellite images are suited to the derivation of low-level AMVs. Reflection of visible radiation from lower clouds is greater than that from the ocean surface, and contrast between lower clouds and the ocean surface is sharp in visible imagery. With infrared bands, lower clouds can be identified in infrared window satellite imagery. Himawari-8/9 low-level AMVs derived from VIS (0.64 μm), SWIR (3.9 μm) and IR (10.4 μm) imagery with heights assigned below 700 hPa are treated to produce ASWinds. Table 2 shows the current specifications of Himawari-8/9 AMVs used for ASWinds.

Figure 1 shows low-level VIS AMVs around Typhoon Ampil overlaid on a Himawari-8 VIS image. Low-level AMVs can be derived by tracking lower clouds in gaps between dense clouds around TCs, where lower clouds are frequently covered with cirrus and rapidly deformed by strong winds or convective activity. Rodgers et al. (1979) and Uchida et al. (1991) showed that the use of satellite imagery with shorter time intervals improves the quantity of low-level AMVs around TCs based on comparison of AMVs from images with 30-, 15- and 7.5-min. intervals. Thus, Himawari-8/9 imagery from high-frequency observation contributes to the quantity of low-level AMVs around TCs.

Himawari-8/9 ASWinds are produced from full-disk and target observation imagery, and are provided to the RSMC Tokyo – Typhoon Center every 30 and 10 min., respectively,

in a binary format that can be handled using JMA's Satellite Animation and Interactive Diagnosis (SATAID) program.

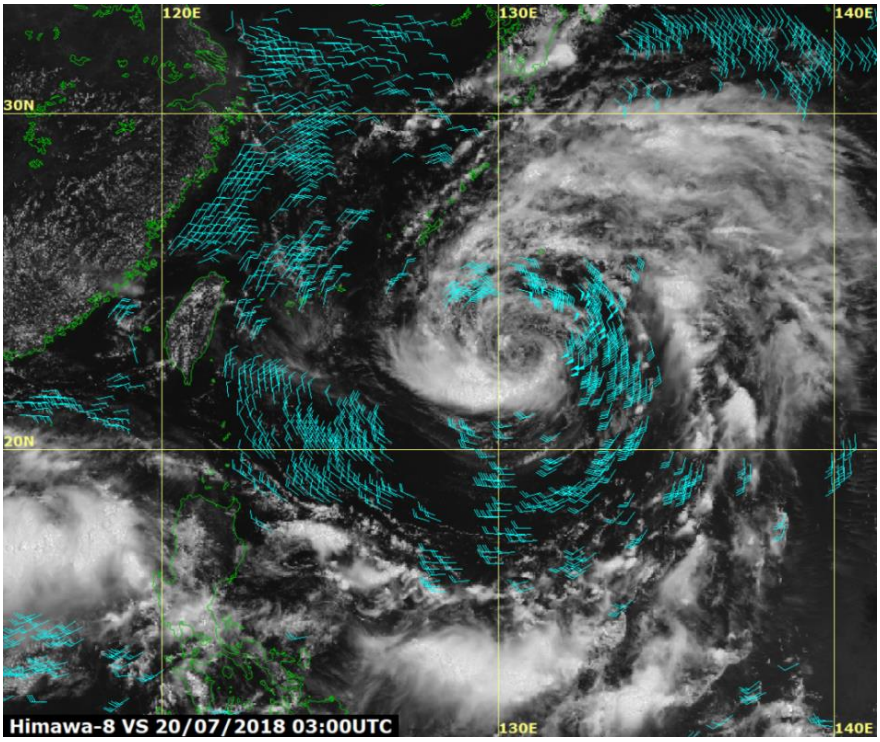

Figure 1. Himawari-8 VIS image and low-level VIS AMVs around Typhoon Ampil at 03 UTC on 20 July 2018

2.2. Estimation of sea surface winds using Himawari-8/9 low-level AMVs

Powell (1980) reported that sea surface winds can be estimated empirically by multiplying low-level aircraft wind values (approx. at 500 m) by 0.8 in a hurricane. Comparison of low-level AMVs derived from MTSAT-1R's special rapid scan imagery with ASCAT winds indicates that the mean speed of ASCAT winds was about 0.8 times that of low-level AMVs up to 15 m/s (Bessho et al. 2016). Figure 2 shows the results of comparison between Himawari-8 low-level VIS AMVs and ASCAT winds as matched up within a radius of 1,000 km from the center of TCs from May to December 2015. A strong correlation is seen between low-level AMVs and ASCAT winds. It was also found that sea surface wind speeds can be estimated from low-level AMVs via multiplication by 0.76 based on linear regression analysis (Nonaka et al. 2016). The factor of 0.76 is similar to the 0.8 value proposed in the previous research discussed above.

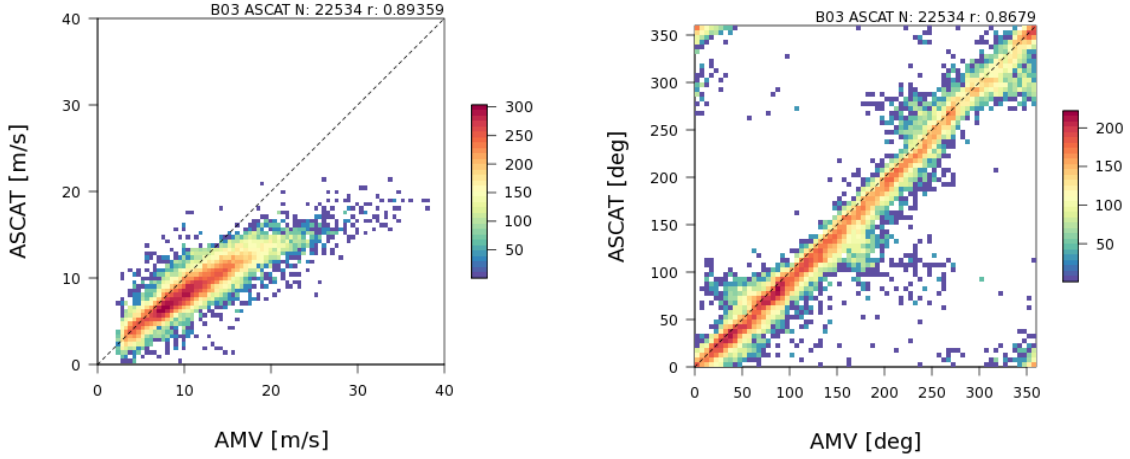

Figure 2. Comparison between Himawari-8 low-level VIS (B03) AMVs and ASCAT winds within a radius of 1,000 km from the center of TCs from May to December 2015 (left: wind speed; right: wind direction) (Nonaka et al. 2016)

The factor of 0.76 is close to the 0.75 wind speed ratio between the surface and the flight level as recommended for the outer vortex region of TCs at 925 hPa by Franklin et al. (2003). The altitude of 925 hPa is also consistent with the assignment of most Himawari-8/9 low-level AMVs around TCs at altitudes below 900 hPa. Figure 2 indicates large wind speed differences between low-level AMVs and ASCAT winds at high wind speeds, indicating possible overestimation of sea surface winds when a constant factor is used. Although the risk of overestimation could be suppressed by using a smaller factor for high wind speeds, a constant factor of 0.76 is initially adopted for ASWinds calculation in the interests of avoiding underestimation.

3. Accuracy and limitations of Himawari-8/9 ASWinds

This chapter reports on the results of validation for Himawari-8 full-disk ASWinds against ASCAT winds around TCs occurring in 2016.

3.1. Data set

ASWinds estimated from full-disk low-level AMVs derived from three spectral bands (VIS, SWIR and IR) were compared with ASCAT winds in the vicinity of TCs occurring in 2016 (T1601 – T1626). The conditions for the match-up between ASCAT winds and ASWinds were as follows:

- Location within 1,000 km of TC centers as determined by hourly interpolation of JMA's 2016 best-track data
- Observation time difference within 15 minutes

- Selection of nearest pair located 0.05° apart or less (in longitude and latitude)

3.2. Comparison of ASWinds and ASCAT winds

3.2.1. Wind speed

Figure 3 shows wind speed correlations of collocated data between ASCAT winds and Himawari-8 full-disk ASWinds. VIS and IR ASWinds correspond closely to ASCAT winds up to approximately 15 m/s.

Table 3 shows statistics on wind speed and direction between ASWinds and ASCAT winds (ASWinds minus ASCAT winds) for each ASWind speed (every 5 m/s). The values are seen to correspond, and the root mean square (RMS) of wind speed differences is 1.2 – 1.7 m/s up to 15 m/s. The wind speed of VIS ASWinds is more consistent with ASCAT winds than that of SWIR and IR ASWinds. In regions of high wind speed (approx. > 15 m/s), RMS differences are large in terms of both wind speed and direction. Positive wind speed biases against ASCAT winds are seen in high wind speed regions in Figure 3, although the number of samples is low.

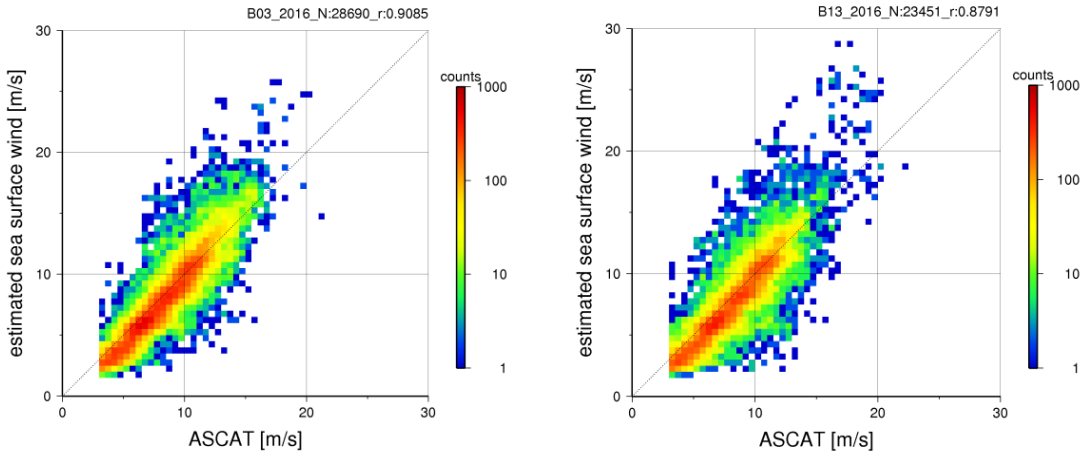

Figure 3. Speed comparison of full-disk VIS ASWinds (left) and IR ASWinds (right) with ASCAT winds. Collocation is within 1,000 km of the center of TCs forming in 2016.

Table 3. Statistics for ASWinds and ASCAT winds around TCs forming in 2016. Note that ASWind direction is not corrected from that of low-level AMVs, and bias represents the relative angle of low-level AMVs against ASCAT winds.

	N	Wind speed [m/s]		Wind direction [°]	
		RMS	Bias	RMS	Bias
B03 (> 5 m/s)	***23,015***	***1.46***	***-0.19***	***13.6***	***7.59***
0 – 5 m/s	5,675	1.41	-1.12	28.8	2.68
5 – 10 m/s	15,685	1.21	-0.64	13.5	6.27
10 – 15 m/s	6,518	1.47	0.49	12.9	9.73
15 – 20 m/s	770	3.57	2.85	18.4	15.6
> 20 m/s	42	7.15	6.83	27.3	25.2
B07 (> 5 m/s)	***20,093***	***1.66***	***-0.21***	***15.8***	***8.58***
0 – 5 m/s	5,447	1.65	-1.22	30.6	2.93
5 – 10 m/s	12,774	1.43	-0.75	15.8	6.91
10 – 15 m/s	6,618	1.53	0.45	14.6	10.5
15 – 20 m/s	598	3.71	2.82	23.4	19.9
> 20 m/s	103	7.18	6.71	29.3	28.1
B13 (> 5 m/s)	***18,233***	***1.68***	***-0.28***	***16.6***	***8.68***
0 – 5 m/s	5,218	1.67	-1.24	31.2	3.10
5 – 10 m/s	12,288	1.46	-0.78	16.8	7.30
10 – 15 m/s	5,434	1.56	0.46	15.0	10.4
15 – 20 m/s	425	4.12	3.22	25.7	22.2
> 20 m/s	86	7.56	7.15	29.1	28.0

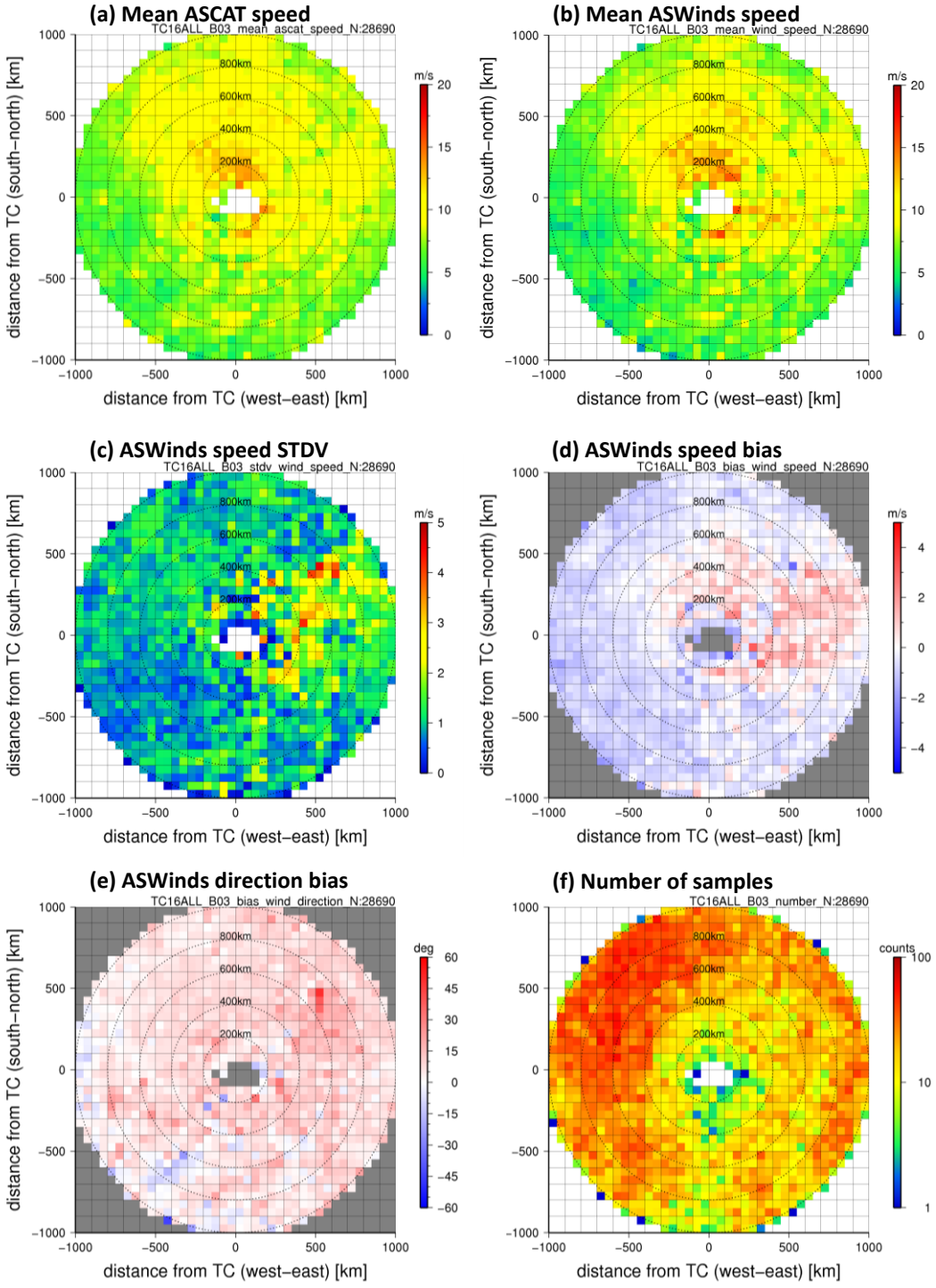

Figure 4. Distribution of statistics for VIS ASWinds and ASCAT winds within 1,000 km of TC centers. (a) mean speed of ASCAT winds, (b) mean speed of ASWinds, (c) standard deviation of ASWinds speed, (d) speed bias of ASWinds, (e) ASWind direction bias, and (f) number of samples. Values were calculated over every 50 × 50 km area for the latitudinal and longitudinal directions within 1,000 km of TC centers.

Figure 4 shows horizontal distributions of statistics for VIS ASWinds and ASCAT winds around TCs as calculated over every 50 × 50 km area for the latitudinal and longitudinal directions within 1,000 km of TC centers. The horizontal distribution of mean wind speed around TCs is similar for both (Figure 4 (a) and (b)), although it should be noted that the sample is relatively small for the eastern part of TCs and within a radius of 400 km from the center as compared to other parts (Figure 4 (f)). In addition, the mean wind speed is relatively high in TC northern and eastern quadrants. This is consistent with the observation that winds in the right half of a circle centered on a TC are generally stronger than those in the left half in the Northern Hemisphere, and the observation that most TCs move westward or northeastward over the western North Pacific. Positive speed biases of ASWinds are seen in the northern and eastern quadrants of TCs where the mean wind speed is relatively high (Figure 4 (a), (b) and (d)).

3.2.2. Wind direction: relationship between low-level AMVs and ASCAT winds

Table 3 shows that ASWinds have positive wind direction biases against ASCAT winds. Although RMS differences between the two are large, the size of the positive biases is around 10° for 5 – 15 m/s. Since ASWinds are not corrected in terms of direction from those of low-level AMVs here, the direction differences indicate relative angles between the directions of low-level AMVs and ASCAT winds, in which clockwise is defined as positive. Hence, positive/negative direction biases in ASWinds have means that low-level AMVs direct farther outward/inward in relation to the center of the TC than ASCAT winds as seen in Figure 5.

Figure 6 shows the AMV assigned height dependency of the number of samples and wind direction differences between low-level AMVs and ASCAT winds. Standard deviations of the wind direction difference are shown as bars in the figure. The wind direction difference (i.e., the relative angle) gradually increases with altitude from +5 to +11°, which is largely consistent with the difference in inflow angles between the surface and other levels below 925 hPa around TCs (4 to 6° radius region) as reported by Frank (1977). Meanwhile, the relative angle is 5 to 10° smaller than that reported for altitudes above 925 hPa.

Since the direction of ASWinds is not corrected from that of low-level AMVs as detailed above, the values have an outward direction bias approximately 5 to 10° toward the TC center. Direction bias correction for ASWinds is currently under consideration; in the meantime, this characteristic should be noted when ASWinds are used in TC analysis.

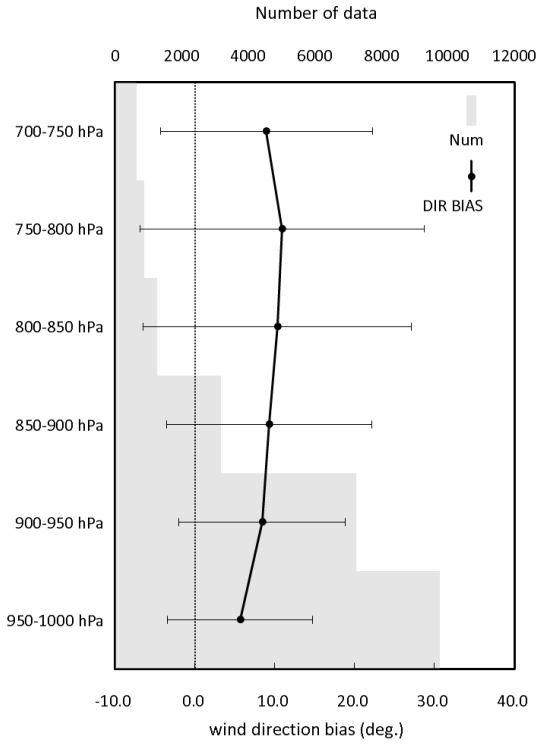

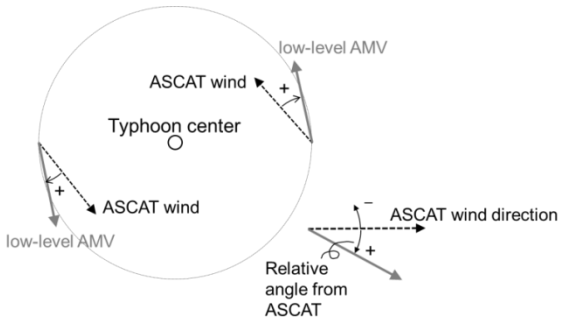

Figure 5. Relationship between directions of low-level AMVs and ASCAT winds

Figure 6. Height dependency of sample number (histogram) and mean wind direction bias (black line and points) of VIS low-level AMVs against ASCAT winds. Bars indicate standard deviations.

3.3. Variation in numbers of ASWinds (low-level AMVs)

As AMV derivation depends on the distribution of cloud patterns and cloud types in satellite imagery, distributions and numbers of derivable ASWinds vary. Figure 7 shows variations in the number of low-level AMVs derived within 1,000 km of the center of Typhoon Nepartak (T1601) from 2 to 10 July 2016. The number of low-level VIS AMVs, which are available only in the daytime, was greater than those of SWIR and IR. Infrared (SWIR and IR) low-level AMVs are also available at night. Himawari-8/9 SWIR AMVs are not derived around sunrise and sunset in each region in satellite imagery, as the observed radiance is contaminated by the reflection of solar radiation. However, SWIR imagery is nonetheless useful because it is more suited for deriving low-level AMVs at night than IR imagery (Dunion and Velden 2002b). In Figure 7, there are more SWIR low-level AMVs than those of IR at night.

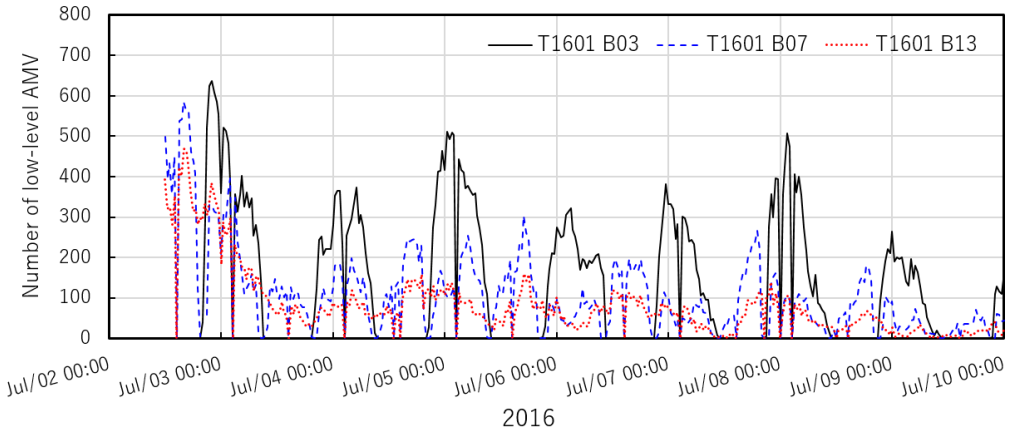

Figure 7. Time-series representation of numbers of Himawari-8 low-level AMVs located within 1,000 km of the center of Typhoon Nepartak (T1601) over a period of approximately a week. VIS (B03) (solid black line), SWIR (B07) (dashed blue line) and IR (B13) (dashed red line).

4. Operational usage for TC monitoring at the RSMC Tokyo – Typhoon Center

In 2017, the RSMC Tokyo – Typhoon Center began monitoring operational application of ASWinds provided by JMA/MSC on a trial basis for periods when TCs are present in its area of responsibility. The trial was ended and routine monitoring was introduced in June 2018.

4.1. Typhoon Lan (T1721)

Figure 8 shows an example of ASWinds for Typhoon Lan (T1721) from 12 to 17 UTC on 22 October 2017. Analysis shows clear large-scale circulation due to the influences of a TC in surrounding areas. Although ASWinds were not estimated in areas with dense clouds, this figure demonstrates the effectiveness of this approach for identifying areas with strong winds.

Figure 9 shows satellite images with ASCAT winds. Scatterometers such as those of ASCAT are advantageous for observation even in areas with relatively dense clouds, but cannot observe areas immediately below the satellite, and the range of coverage is zonal which is narrower than that of ASWinds from Himawari-8. In addition, as ASCAT observation is conducted twice a day, only data for 12 and 13 UTC from Metop-B and A, respectively, are obtained, while more data are available for ASWinds from Himawari-8.

In this way, both ASWinds and ASCAT winds have pros and cons. On the pro side, ASWinds are very useful for their high frequency and wider coverage, while ASCAT winds are effective for determining sea surface wind data even in areas with dense clouds. Accordingly, the RSMC Tokyo – Typhoon Center operationally uses ASWinds with any available ASCAT winds overlaid (Figure 10). Comparison of these data also enables

verification of ASWinds accuracy.

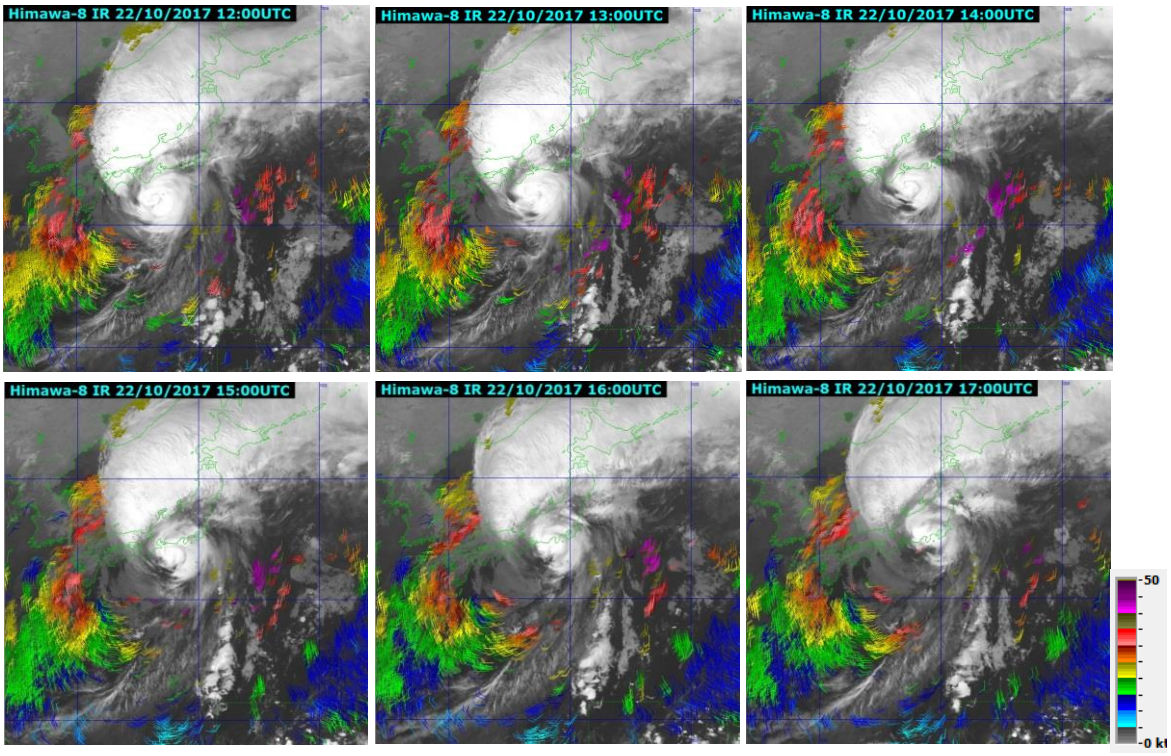

Figure 8. ASWinds from full-disk observation for Typhoon Lan (T1721) from 12 to 17 UTC on 22 October 2017. Wind speed symbols in brown or purple indicate values of 35 kt or higher.

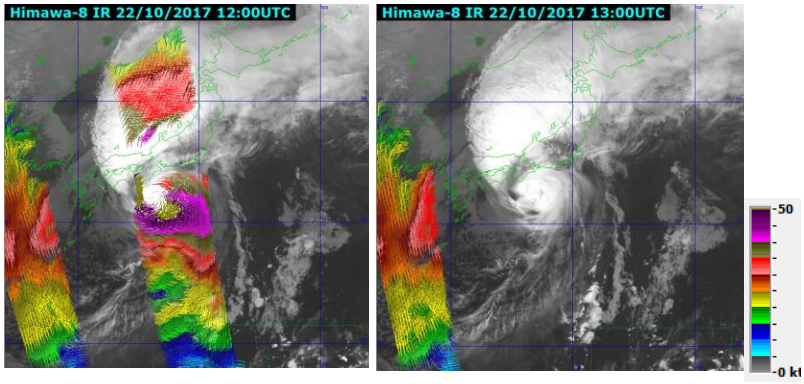

Figure 9. Satellite images with sea surface winds derived from ASCAT for Typhoon Lan (T1721) from 12 to 17 UTC on 22 October 2017. As ASCAT observation is conducted twice a day, two images at 12 UTC from Metop-B (left) and at 13 UTC from Metop-A (right) were obtained.

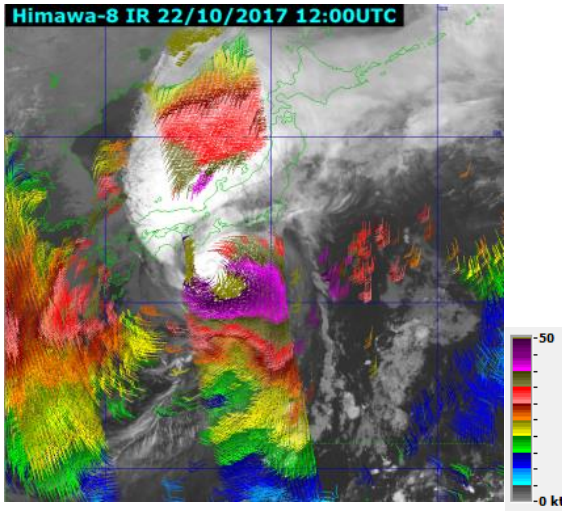

Figure 10. ASWinds from full-disk observation for Typhoon Lan (T1721) at 12 UTC on 22 October 2017 with ASCAT winds overlaid

4.2. Tropical depression in the eastern Philippines

In late December 2018, a tropical depression formed in the eastern Philippines and was expected to become a tropical storm, although it eventually did not. The RSMC Tokyo – Typhoon Center began detailed analysis of the system at 12 UTC on 25 December. ASWinds (especially those from target observation) proved effective in estimating the center position as well as clarifying strong wind distribution and determining the stage of development.

Figure 11 shows satellite imagery from 15 UTC on December 26. The cloud system center (CSC) was apparently located somewhere in a dense cloud extending from around 9 to 13°N and from 127 to 131°E in Himawari-8 IR imagery. However, ASWinds revealed that the CSC was outside the dense cloud area. As VIS imagery was not available for 15 UTC, IR ASWinds played an important role in center position estimation, and those from target observation made a particularly significant contribution. As seen in Figure 11, ASWinds from target observation pointed to the center at around 10°N, 131°E, while the center position and areas with strong winds were not readily identifiable in ASWinds from full-disk observation.

Twelve hours later at 03 UTC (Figure 12), VIS ASWinds again revealed a center position outside the dense cloud area at around 10°N, 130 – 131°E. At this time, available VIS imagery showed circulation at around the same center position as seen from ASWinds. Although this position was identified in ASWinds from full-disk observation slightly more clearly than 12 hours before, target observation still provided better information. ASWinds from target observation also indicated that the system was stronger with winds at speeds up to around 25 kt.

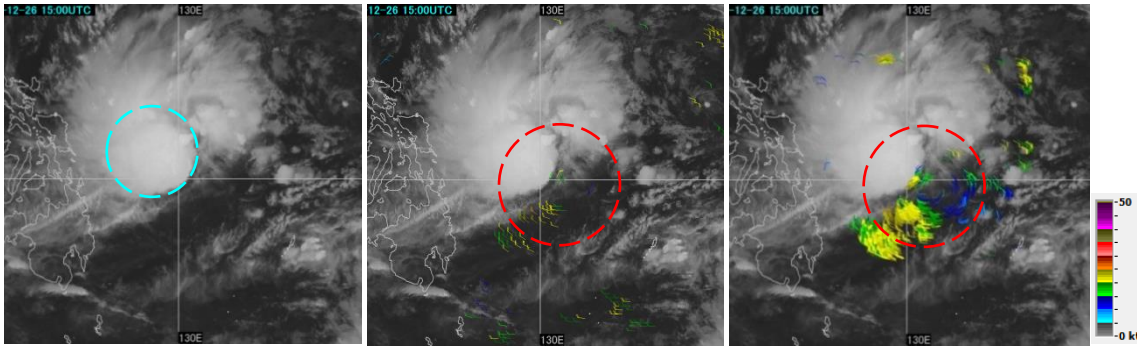

Figure 11. IR (B13) image (left), ASWinds from full-disk observation (middle) and ASWinds from target observation (right) at 15 UTC on 26 December 2018. The dashed blue circle shows the area in which the CSC is apparently located. The dashed red circle indicates the area around the actual center position with winds at speeds of 25 kt or higher.

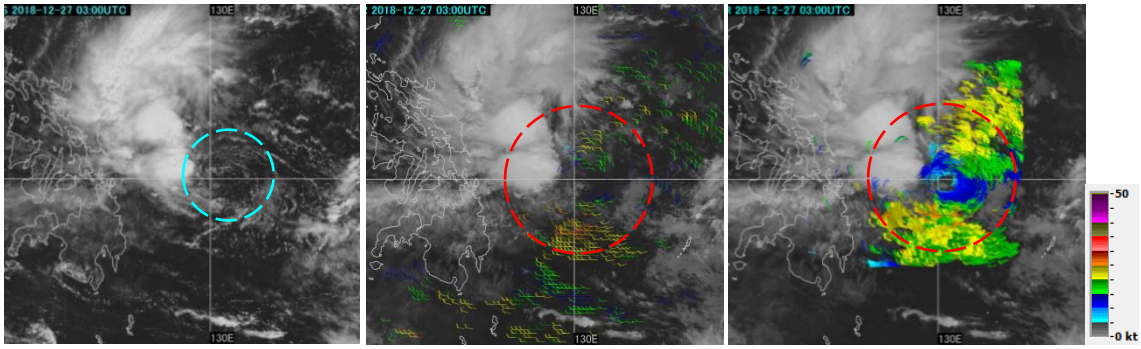

Figure 12. VIS (B03) image (left) and ASWinds (right) at 03 UTC on 27 December 2018. The dashed blue circle shows the area where circulation was observed. The dashed red circle indicates the area around the actual center position with winds at speeds of 25 kt or higher.

5. Summary

The quality and quantity of Himawari-8/9 AMVs have been improved via the use of Himawari-8/9's high-frequency and multi-spectral band observation imagery along with the specified AMV derivation algorithm. Himawari-8/9 ASWinds (i.e., sea surface wind data estimated from low-level AMVs) have been utilized at the RSMC Tokyo – Typhoon Center since July 2017 as a valuable source of wind information for TC analysis.

Himawari-8/9 full-disk ASWinds were validated for areas around TCs occurring in 2016 based on comparison with ASCAT winds. The RMS difference of the wind speed was 1.4 to 1.7 m/s, and Himawari-8/9 ASWinds were found to correspond closely to ASCAT winds below around 15 m/s. Meanwhile, Himawari-8/9 ASWinds were found to have a positive speed bias (3 – 7 m/s) in the high wind speed region (> 15 m/s) as well as a wind direction bias (up to around 10°). A method involving the use of AMV height information to reduce these biases is currently being researched.

Himawari-8/9 ASWinds provide more detailed wind information for areas around TCs based on the use of low-level AMVs derived from target observation than those from full-disk observation. Use of the resulting data, which are provided every 10 min., has also proven effective.

Himawari-8/9 ASWinds from full-disk and target observation are currently used only by the RSMC Tokyo – Typhoon Center for its own operations, but are scheduled for widespread distribution in the near future to support TC monitoring operations.

References

Bessho, K., K. Date, M. Hayashi, A. Ikeda, T. Imai, H. Inoue, Y. Kumagai, T. Miyakawa, H. Murata, T. Ohno, A. Okuyama, R. Oyama, Y. Sasaki, Y. Shimazu, K. Shimoji, Y. Sumida, M. Suzuki, H. Taniguchi, H. Tsuchiyama, D. Uesawa, H. Yokota, and R. Yoshida, 2016: An Introduction to Himawari-8/9 – Japan's New-Generation Geostationary Meteorological Satellites. *J. Meteor. Soc. Japan*, **94**, 151-183.

Dunion, J. P., and C. S. Velden, 2002a: Application of Surface-Adjusted GOES Low-Level Cloud-Drift Winds in the Environment of Atlantic Tropical Cyclones. Part I: Methodology and Validation. *Mon. Wea. Rev.*, **130**, 1333-1346.

Dunion, J. P., and C. S. Velden, 2002b: Using The GOES 3.9 μm Shortwave Infrared Channel to Track Low-level Cloud-drift Winds. *Proc. of 6th International Winds Workshop.* [Available at http://cimss.ssec.wisc.edu/iwwg/iww6/session6/Dunion_1.pdf.]

Frank, W. M., 1977: The Structure and Energetics of the Tropical Cyclone I. Storm Structure. *Mon. Wea. Rev.*, **105**, 1119-1135.

Franklin, J. L., M. L. Black, and K. Valde, 2003: GPS Dropsonde Wind Profiles in Hurricanes and Their Operational Implications. *Wea. Forecasting*, **18**, 32-43.

Holmlund, K., 1998: The utilization of statistical properties of satellite-derived atmospheric motion vectors to derive quality indicators. *Wea. Forecasting*, **13**, 1093-1104.

Nonaka, K., K. Shimoji, and K. Kato, 2016: Estimation of The Sea Surface Wind in The Vicinity of Typhoon using Himawari-8 Low-Level AMVs. *Proc. of 13th International Winds Workshop.* [Available at http://cimss.ssec.wisc.edu/iwwg/iww13/proceedings_iww13/papers/session6/IWW13_Session6_4_Nonaka_final_update.pdf.]

Ohshima, T., H. Uchida, T. Hamada, and S. Osano, 1991: A comparison of GMS cloud motion winds with ship-observed winds in typhoon vicinity. *Geophys. Mag.*, **44**, 27-36.

OSI SAF/EARS, ASCAT Wind Product User Manual (2016).

http://projects.knmi.nl/scatterometer/old_manuals/ss3_pm_ascat_1.14.pdf

Powell, M. D., 1980: Evaluation of Diagnostic Boundary-Layer Models Applied to Hurricanes. *Mon. Wea. Rev.*, **108**, 757-766.

Shimoji, K., 2017: Introduction to the Himawari-8 Atmospheric Motion Vector Algorithm. *Meteorological Satellite Center technical note*, **62**, 73-77.